

ISSN: (Print) (Online) Journal homepage: www.tandfonline.com/journals/tbsd20

Predicting anti-COVID-19 potential: in silico analysis of Mauritine compound from *Ziziphus-spina christi* as a promising papain-like protease (PLpro) inhibitor

Taufik Muhammad Fakhri, Fitrianti Darusman, Riry Apriliani, Syifa Prahayati, Dwi Syah Fitra Ramadhan, Aulia Fikri Hidayat, Aden Dhana Rizkita & Tegar Achsendo Yuniarta

To cite this article: Taufik Muhammad Fakhri, Fitrianti Darusman, Riry Apriliani, Syifa Prahayati, Dwi Syah Fitra Ramadhan, Aulia Fikri Hidayat, Aden Dhana Rizkita & Tegar Achsendo Yuniarta (26 Mar 2024): Predicting anti-COVID-19 potential: in silico analysis of Mauritine compound from *Ziziphus-spina christi* as a promising papain-like protease (PLpro) inhibitor, Journal of Biomolecular Structure and Dynamics, DOI: [10.1080/07391102.2024.2322627](https://doi.org/10.1080/07391102.2024.2322627)

To link to this article: <https://doi.org/10.1080/07391102.2024.2322627>



Published online: 26 Mar 2024.



Submit your article to this journal [↗](#)








View related articles [↗](#)



View Crossmark data [↗](#)



Predicting anti-COVID-19 potential: in silico analysis of Mauritian compound from *Ziziphus-spina christi* as a promising papain-like protease (PLpro) inhibitor

Taufik Muhammad Fakhri^a , Fitrianti Darusman^{a,b} , Riry Apriliani^a, Syifa Prahayati^a, Dwi Syah Fitra Ramadhan^c , Aulia Fikri Hidayat^a , Aden Dhana Rizkita^{d,e} , and Tegar Achsendo Yuniarta^f 

^aDepartment of Pharmacy, Faculty of Mathematics and Natural Sciences, Universitas Islam Bandung, Bandung, Indonesia; ^bDepartment of Pharmaceutics and Pharmaceutical Technology, Faculty of Pharmacy, Universitas Padjadjaran, Bandung, Indonesia; ^cDepartment of Pharmacy, Poltekkes Kemenkes Makassar, Makassar, Indonesia; ^dDepartment of Pharmacy, Sekolah Tinggi Ilmu Kesehatan (STIKES) Bogor Husada, Bogor, Indonesia; ^eSchool of Pharmacy, College of Pharmacy, Taipei Medical University, Taipei, Taiwan; ^fDepartment of Pharmaceutical Chemistry, Faculty of Pharmacy, University of Surabaya, Surabaya, Indonesia

Communicated by Ramaswamy H. Sarma

ABSTRACT

The COVID-19 pandemic caused by the SARS-CoV-2 virus, recognized by the World Health Organization (WHO), has led to 164,523,894 confirmed cases and 3,412,032 deaths globally as of May 20, 2021. SARS-CoV-2 encodes crucial proteases for its replication cycle, including the papain-like protease (PLpro), presenting a potential target for developing COVID-19 treatments. Mauritian, a cyclopeptide alkaloid found in the *Ziziphus-spina christi* plant, exhibits antiviral properties and was investigated for its affinity and toxicity towards PLpro using molecular docking through MGLTools 1.5.6 with Autodock Tools 4.2. Preceding this, toxicity and ADME prediction were performed via Toxtree 3.1.0 software and SwissADME servers. Results from molecular docking revealed free binding energy values of -8.58 ; -7.73 ; -8.36 ; -6.07 ; -6.67 ; -7.83 ; -7.67 ; -7.40 ; and -6.87 Kcal/mol for Mauritian-A, Mauritian-B, Mauritian-C, Mauritian-D, Mauritian-F, Mauritian-H, Mauritian-J, Mauritian-L, and Mauritian-M, respectively. Correspondingly, inhibition constants were 0.51724; 2.14; 0.7398; 35.43; 12.95; 1.83; 2.38; 3.80; and 9.17 μ M, respectively. Interactions observed included hydrogen bonds, hydrophobic interactions, and electrostatic interactions between the Mauritian compounds and the receptor. Mauritian-A and Mauritian-C emerged as a promising anti-COVID-19 candidate due to its superior affinity compared to other derivatives, as indicated by research findings. Interestingly, Mauritian-A and Mauritian-C exhibits notable stability as depicted by the RMSD and RMSF graphs, along with a considerable MM-PBSA binding free energy value of -162.431 and -137.500 kJ/mol, respectively.

ARTICLE HISTORY

Received 28 November 2023
Accepted 19 February 2024

KEYWORDS

In silico approach; papain-like protease (PLpro); COVID-19; Mauritian; *Ziziphus-spina christi*

1. Introduction

Since its inception in December 2019 in Wuhan, China, the novel coronavirus has triggered a swift propagation of coronavirus disease 2019 (COVID-19) (Guo et al., 2020; Yang & Yang, 2020). Owing to its swift transmission across diverse nations, the World Health Organization (WHO) declared COVID-19 a pandemic on March 11, 2020 (Mohamed et al., 2022). COVID-19 stems from SARS-CoV-2 infection and has been formally designated as Severe Acute Respiratory Syndrome Coronavirus-2 (SARS-CoV-2) by the International Committee on Taxonomy of Viruses (ICTV). As per the World Health Organization's report until May 20, 2021, there were 164,523,894 confirmed COVID-19 cases worldwide, resulting in 3,412,032 fatalities (Kidaka et al., 2020; Liu et al., 2021). The COVID-19 outbreak has emerged as a significant global health crisis in recent decades, profoundly impacting human existence and emphasizing the urgency for enhanced response measures.

SARS-CoV-2, a non-segmented RNA virus, aligns with the new β -coronavirus category, succeeding predecessors like

SARS-CoV and MERS-CoV, which instigated outbreaks primarily in Guangdong, China, and Saudi Arabia (Moreno-Eutimio et al., 2020). Through extensive genome analyses, the resemblance between SARS-CoV-2 and SARS-CoV has been well-documented (Li et al., 2020). Research into COVID-19 strongly suggests bats as the potential primary reservoir for this virus, with the genome of SARS-CoV-2 exhibiting a striking 96.2% similarity to the bat coronavirus RaTG13 (Anand et al., 2020; Velayati et al., 2020). Its structure comprises four fundamental structural proteins: spike (S), envelope (E), membrane (M), and nucleocapsid (N). The spike proteins on SARS-CoV-2 serve as the key for entering host cells, binding to specific receptors on the cell surface (Walls et al., 2020).

SARS-CoV-2 harbors two critical proteases, integral to its replication mechanism: the papain-like protease (PLpro, encoded in Nsp3) and the chymotrypsin-like main protease (3CLpro or Mpro, encoded in Nsp5) (Sokolinskaya et al., 2022). These proteases work collaboratively to process viral polyproteins (pp1a and pp1b). Within Nsp3, PLpro stands as a multifaceted protein, playing a pivotal role in cleaving and refining viral polyproteins, orchestrating the assembly of the

replicase-transcriptase complex (RTC), and exerting suppressive effects on the host's immune response (Armstrong et al., 2021; Yang et al., 2014). Given its fundamental contribution to viral replication, PLpro emerges as an appealing target in the ongoing exploration for potential antiviral therapeutic interventions (Arya et al., 2022). Understanding the intricacies of PLpro's function presents a promising avenue in the development of strategies aimed at combating SARS-CoV-2 and curbing the progression of COVID-19 (Bhowmick et al., 2022).

In the pursuit of identifying potential treatments for COVID-19, various compounds sourced from medicinal plants have undergone computational testing against SARS-CoV-2. One promising plant for therapeutic purposes is the Arabian bidara (*Ziziphus spina-christi*) plant, recognized for its presence of significant compounds like flavonoids, polyphenols, terpenoids, saponins, glycosides, carbohydrates, and resins (Fakih et al., 2022; Mulyani et al., 2021). Furthermore, several cyclopeptide alkaloids, including Zizyphine-F, Mauritine-C, Jubanine-A, and Amphibine-H, were previously discovered and isolated from the bark of the Arabian bidara plant (Tuenter et al., 2017). This investigation sets the stage for potentially uncovering natural compounds that could serve as a foundation for the development of more efficient therapies in combating the challenges posed by COVID-19 (Farooq Wali et al., 2022; Taghipour et al., 2020). Integrating these natural compounds derived from plant sources may hold considerable promise as a focal point in exploring novel and innovative treatment possibilities.

Cyclopeptide alkaloids, characterized by macrocyclic structures containing rings comprising 13, 14, or 15 members, are predominantly found in Rhamnaceae plants, notably within the *Ziziphus* genus (Adam et al., 2023). These alkaloids boast diverse biological functionalities encompassing antiviral, antibacterial, antifungal, antimalarial properties, and even demonstrate sedative effects (Sakna et al., 2019). This study aims to conduct *in silico* testing utilizing the molecular docking method to evaluate the antiviral potential of the Mauritine compound. By doing so, the research endeavors to yield valuable scientific insights into the prospective antiviral effects of this cyclopeptide alkaloid, potentially offering implications for COVID-19 therapy.

2. Materials and methods

2.1. Instruments and materials

The utilized equipment comprises a collection of high-performance computers (HPC), including an Intel(R) Core i5-8500 CPU @ 4.30 GHz (6 CPUs) processor, 4096 MB RAM, a 2TB hard drive, 120GB solid-state drive, and an NVIDIA GeForce GTX 1080 Ti graphics card. These HPCs are equipped with various software, namely SWISS-ADME server, Quantum ESPRESSO v.6.6, Toxtree 3.1.0, HyperChem 8.0, MGLTools 1.5.6 integrated with AutoDock Tools 4.2, Biovia Discovery Studio 2019, Gromacs 2016.3, and g_mmpbsa package. The materials encompass two-dimensional and three-dimensional structures of Mauritine derivative compounds downloaded via the Pubchem (<https://pubchem.ncbi.nlm.nih.gov/>) database (Figure 1) (Kim et al., 2023). Furthermore,

the macromolecular structure of the papain-like protease receptor (PLpro), obtained from the Protein Data Bank (PDB) (<https://www.rcsb.org/>) website, is also part of the utilized resources.

2.2. Analysis of the ADME Profiles of the Mauritine compounds

The ADME profile assessment (Absorption, Distribution, Metabolism, and Excretion) of the Mauritine compound derivatives was conducted using the SWISS-ADME server (<https://www.swissadme.ch/>) to explore the pharmacological and pharmacokinetic attributes of the Mauritine compounds (Daina et al., 2017). As per Lipinski's rules, the criteria for a potential drug encompass specific parameters: a molecular mass below 500 daltons, considerable lipophilicity (indicated by a log P value below 5), fewer than 5 hydrogen bonds, fewer than 10 bond acceptors, and a molar refractivity ranging between 40 and 130 (Karami et al., 2022).

2.3. Forecasting the toxicity levels of the Mauritine compounds

Toxicity assessments for the Mauritine compounds were conducted through the utilization of Toxtree 3.1.0 software (Yeni et al., 2018). This toxicity prediction process involves evaluating three distinct parameters: Cramer Rules, Kroes TTC, and Carcinogenicity. The Cramer Rules parameter assesses toxicity levels based on functional groups present in the compound, while Kroes TTC estimates the exposure threshold for drug compounds in human subjects. The Carcinogenicity parameter determines whether the compound exhibits negative genotoxic or negative non-genotoxic characteristics.

2.4. Refinement of the geometric structure of Mauritine compounds

Quantum ESPRESSO v.6.6 software was employed to conduct geometry optimization on the Mauritine compound derivative (Giannozzi et al., 2020). This optimization process is aimed at acquiring the precise structural confirmation utilizing the Density Functional Theory (DFT) method employing a 3-21 G basis set (Shen et al., 2012).

2.5. Preparation of macromolecular PLpro receptor structures

The utilized macromolecular structure is the papain-like protease receptor (PLpro) with the PDB code 7CMD, obtained from the Protein Data Bank (PDB) website at <https://www.rcsb.org/structure/7CMD> (Gao et al., 2021). Subsequently, the macromolecules were processed using Biovia Discovery Studio 2019 software, involving steps such as eliminating water molecules, segregating natural ligands from macromolecules, followed by the addition of hydrogen atoms and partial charges (BIOVIA, 2017).

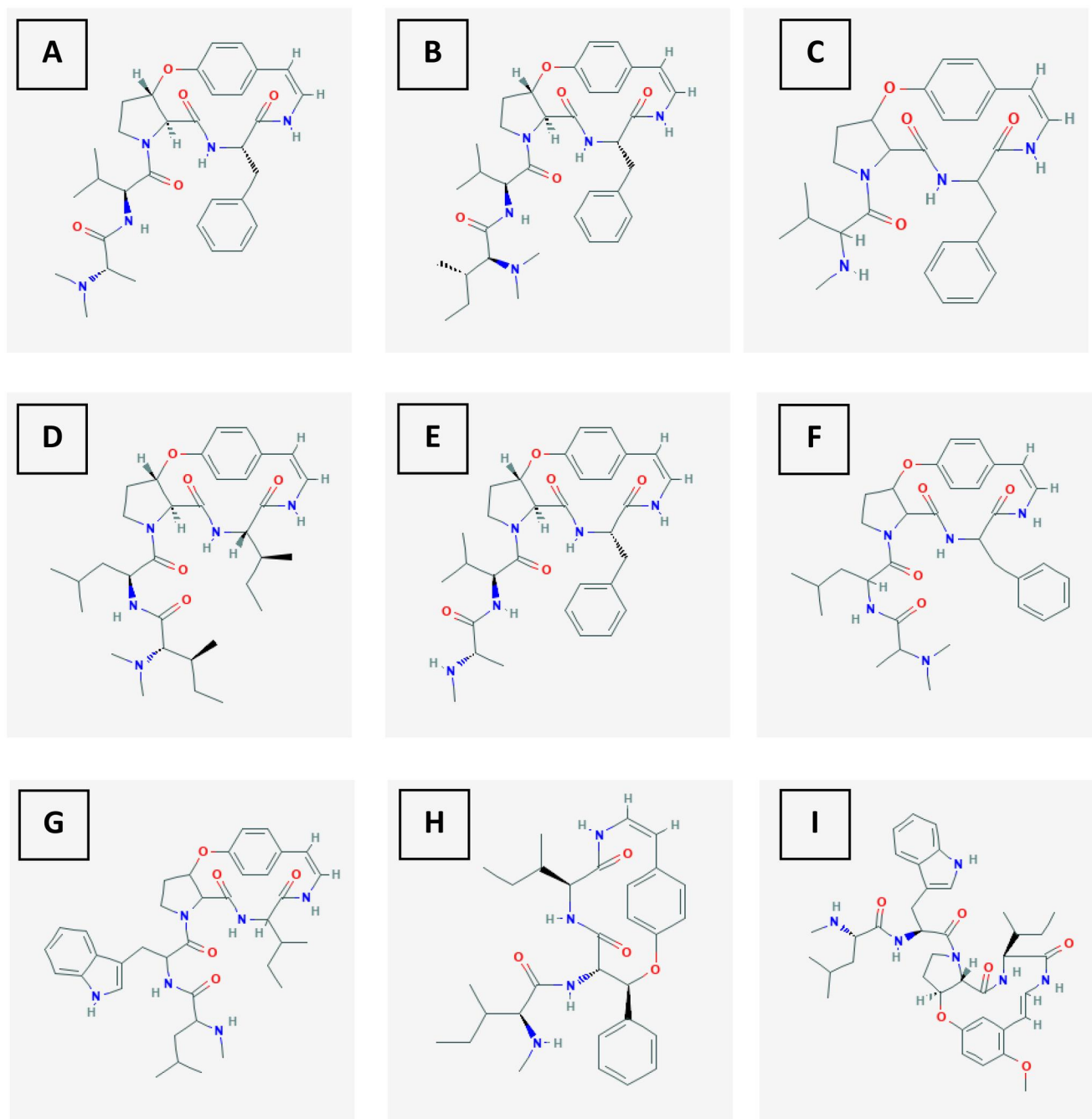


Figure 1. The compounds Mauritine-A (A), Mauritine-B (B), Mauritine-C (C), Mauritine-D (D), Mauritine-F (E), Mauritine-H (F), Mauritine-J (G), Mauritine-L (H), and Mauritine-M (I) depicted in two-dimensional form.

2.6. Validation of the molecular docking method

The validation of the docking procedure involved re-docking the natural ligand to the PLpro receptor utilizing MGLTools 1.5.6 software, coupled with AutoDock Tools 4.2 (Forli et al., 2012). The assessment relied on Root Mean Square Deviation (RMSD) calculations, where a method was deemed valid if the RMSD value was $\leq 2 \text{ \AA}$ (Tallei et al., 2021; Tsai et al., 2023).

2.7. Simulation of molecular docking for Mauritine compounds

Molecular docking simulations involving the PLpro receptor and the Mauritine compound were conducted employing

MGLTools 1.5.6 software, integrated with AutoDock Tools 4.2 (Forli et al., 2012). The objective of this docking simulation was to forecast the binding configuration of a small molecule to its designated target receptor structure, while also comparing the inhibition constant (K_i) and the binding free energy (ΔG) (Djajadisastra et al., 2017; Khan et al., 2022).

2.8. Evaluation of the outcomes from the molecular docking simulations

The examination of the molecular docking outcomes was conducted through Biovia Discovery Studio 2019 software (BIOVIA, 2017). The analysis of the molecular docking data

Table 1. Assessment of the ADME profile of the Mauratine compounds, coupled with the application of Lipinski's rule.

Compound	Molecular weight (g/mol)	Num. H-bond acceptors	Num. H-bond donors	Molar Refractivity	Log P _{o/w} (iLOGP)	Log S (ESOL)	Lipinski
Mauratine-A	575.70	6	3	171.75	3.57	-5.31	Yes; 1 violation: MW > 500
Mauratine-B	617.78	6	3	186.17	3.62	-6.25	Yes; 1 violation: MW > 500
Mauratine-C	490.59	5	3	149.42	3.41	-4.88	Yes; 0 violation
Mauratine-D	597.79	6	3	180.91	4.22	-6.03	Yes; 1 violation: MW > 500
Mauratine-F	561.67	6	4	166.84	3.25	-4.93	Yes; 1 violation: MW > 500
Mauratine-H	589.73	6	3	176.55	3.26	-5.55	Yes; 1 violation: MW > 500
Mauratine-J	656.81	6	5	197.93	3.80	-6.48	No; 2 violation: MW > 500, NorO > 10
Mauratine-L	520.66	5	4	157.14	3.64	-5.63	Yes; 1 violation: MW > 500
Mauratine-M	686.84	7	5	204.42	3.79	-6.57	No; 2 violation: MW > 500, NorO > 10

revealed interactions occurring at the active binding site, specifically highlighting the interactions between the PLpro receptor and the Mauratine compound.

2.9. Simulation of molecular dynamics for Mauratine compounds

The most favorable binding energy compounds, Mauratine-A and Mauratine-C, underwent molecular dynamics simulations spanning 500 nanoseconds of MD production (with a 2 femtosecond timestep). Gromacs 2016.3 software (Abraham et al., 2015; Aragonés et al., 2013), employing the AMBER99SB-ILDN force field (Smith et al., 2015), was utilized for these simulations. Ligand topology and parameters were established using AnteChamber PYthon Parser interface (ACYPPE) (Sousa Da Silva & Vranken, 2012). Electrostatic forces at a distance were determined using the Particle Mesh Ewald (PME) method. Solvation was achieved through the TIP3P water cube model, and system neutralization was accomplished by introducing Sodium and Chloride ions. The system's neutralization employed the autoionize function to add ions sufficient for neutralizing the system. The simulation preparation encompassed a sequence starting with minimization, followed by heating to 310 K, temperature and pressure equilibration stages, culminating in the simulation process. Post-simulation, Root Mean Square Deviation (RMSD) and Root Mean Square Fluctuation (RMSF) analyses were performed to evaluate system stability.

2.10. Calculation of binding free energy using MM-PBSA

Additionally, the computation of binding free energy was executed using the MM-PBSA method (Ren et al., 2020; Wang et al., 2017). This process was conducted through the g_mmpbsa package, integrated within the Gromacs 2016.3 software. In accordance with the MM-PBSA method, the binding free energy (ΔG_{bind}) of the complex is derived from the variance between the free energies of the complex ($\Delta G_{\text{complex}}$) and the unbound receptor (ΔG_{rec}), along with the free ligand (ΔG_{lig}). The Poisson-Boltzmann equation was employed to calculate the polar desolvation energy, utilizing a grid size set at 0.5 Å. The solvent dielectric constant was designated as 80, simulating water as the solvent medium. The nonpolar contribution was determined by the solvent-accessible surface area, defined by a solvent radius of 1.4 Å. Assessments of the complexes' binding free energy were

based on data derived from molecular dynamics simulations, utilizing 500 snapshots extracted from 1 to 500 nanoseconds of simulation trajectories.

3. Results and discussions

3.1. Analysis of the ADME profiles of the Mauratine compounds

Prior to conducting the molecular docking simulation, the physicochemical attributes of the Mauratine compound were initially evaluated to discern the compound's pharmacokinetic and pharmacological traits. This assessment was facilitated through the SWISS-ADME server, leveraging Lipinski's rules as a basis for observation. Lipinski's rule, also recognized as Lipinski's Rule of Five, serves as a guideline to predict compounds with limited permeation and absorption capabilities. The rule primarily addresses a compound's solubility and its ability to permeate biological membranes via passive diffusion. According to Lipinski's rule, compounds tend to exhibit reduced permeation and absorption capacities if their molecular weight exceeds 500, if they possess more than five hydrogen bond donors, if the hydrogen bond acceptors exceed ten, and if the log P or lipophilicity value surpasses 5.

Based on the ADME profile outlined in Table 1, the compounds Mauratine-J and Mauratine-M fail to comply with Lipinski's rule due to their molecular weights surpassing 500 g/mol. A higher molecular weight in a drug signifies a larger molecular size, potentially impeding its ability to permeate biological membranes and prolonging the drug's absorption duration within the body (Muchtaridi et al., 2023). However, across all Mauratine compounds, the count of hydrogen bond donors and acceptors adheres to Lipinski's rule criteria, as they exhibit fewer than five hydrogen bond donors and fewer than ten hydrogen bond acceptors. The quantity of hydrogen bond donors and acceptors significantly influences a drug's biological activity, as these bonds can impact various physicochemical properties of drugs, including melting and boiling points, water solubility, chelate formation capacity, and acidity (Kumar et al., 2023). Moreover, a higher count of hydrogen bond donors and acceptors indicates a heightened hydrogen bond capacity, consequently demanding more energy for the absorption process to occur (Lohidakshan et al., 2018).

Additionally, the molar refractivity values for all Mauratine compounds deviate from the required range specified in the

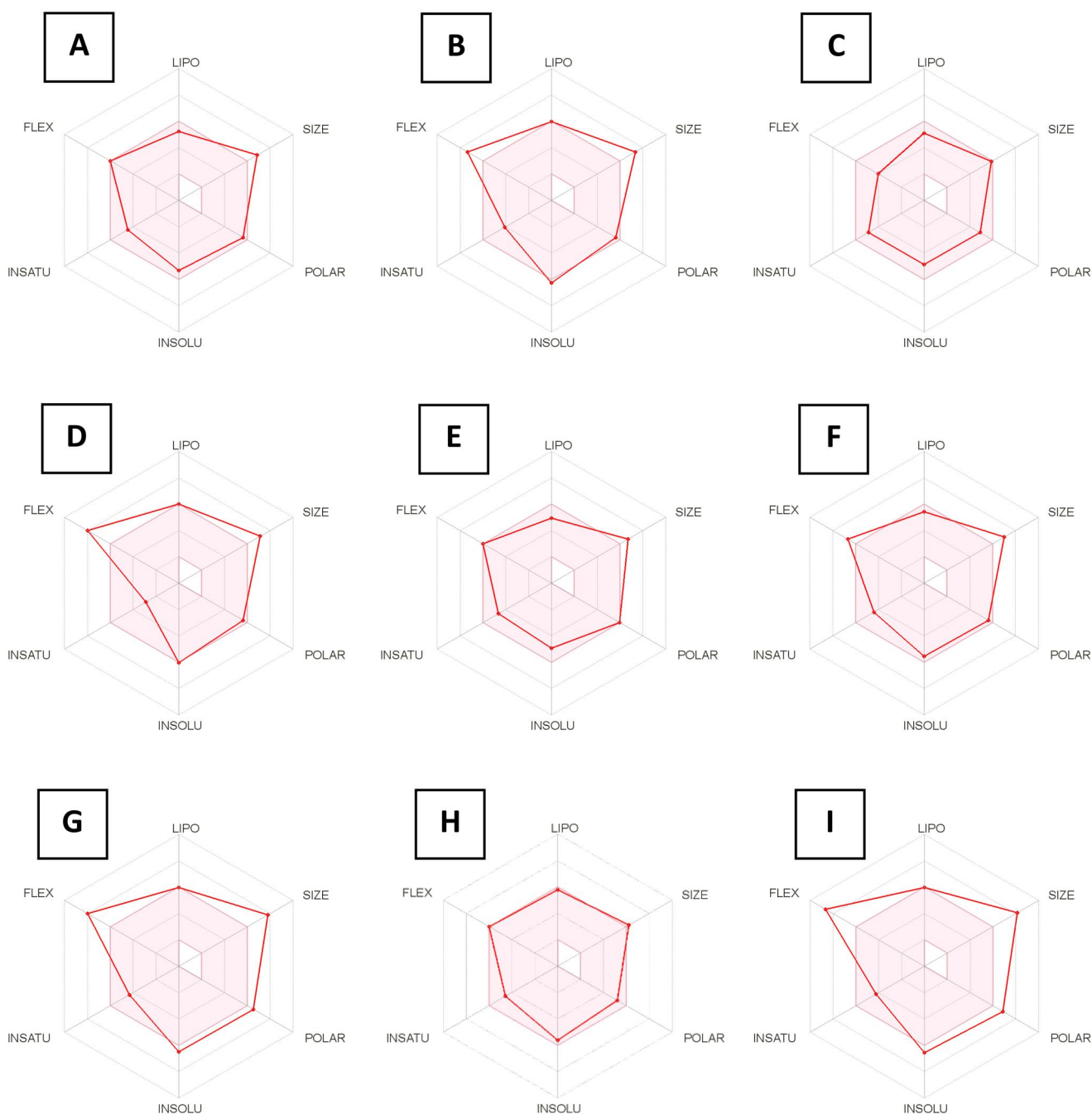


Figure 2. Radar chart depicting the ADME profiles of compounds Mauristine-A (A), Mauristine-B (B), Mauristine-C (C), Mauristine-D (D), Mauristine-F (E), Mauristine-H (F), Mauristine-J (G), Mauristine-L (H), and Mauristine-M (I).

Lipinski rule for calculated molar refractivity (CMR), as they fall outside the 40-130 range (Kumar et al., 2021). Elevated CMR values correspond to increased steric effects, potentially resulting in less favorable interactions between the drug and its receptor. However, the log P value for all Mauristine compounds aligns with Lipinski's rule, exhibiting log P value below 5. This parameter signifies the compound's lipophilicity, indicating its ability to dissolve in lipids. Higher log P value suggest increased hydrophobicity, leading to prolonged retention within the lipid bilayer and wider distribution in the body, potentially reducing binding selectivity to the target enzyme (Az-Zahra et al., 2022). Moreover, excessively negative log P value might hinder molecules from

effectively passing through biological membranes. This is further supported by Figure 2, displaying predictions for six ADME parameters closely associated with a compound's oral bioavailability: LIPO (lipophilicity), SIZE (size), POLAR (polarity), INSOLU (insolubility), INSATU (instauration), and FLEX (flexibility). The color-coded zones represent physicochemical regions conducive to oral bioavailability.

3.2. Forecasting the toxicity levels of the Mauristine compounds

To assess the toxicity of the Mauristine compound, Toxtree 3.1.0 software was employed to predict potential toxic

Table 2. Forecasting the toxicity of the Mauritine compounds.

Compound	Cramer rules	Kroes TTC	Carcinogenicity
Mauritine-A	High Class III	Substance would not be expected to be a safety concern	Negative for nongenotoxic carcinogenicity
Mauritine-B	High Class III	Substance would not be expected to be a safety concern	Negative for nongenotoxic carcinogenicity
Mauritine-C	High Class III	Substance would not be expected to be a safety concern	Negative for nongenotoxic carcinogenicity
Mauritine-D	High Class III	Substance would not be expected to be a safety concern	Negative for nongenotoxic carcinogenicity
Mauritine-F	High Class III	Substance would not be expected to be a safety concern	Negative for nongenotoxic carcinogenicity
Mauritine-H	High Class III	Substance would not be expected to be a safety concern	Negative for nongenotoxic carcinogenicity
Mauritine-J	High Class III	Substance would not be expected to be a safety concern	Negative for nongenotoxic carcinogenicity
Mauritine-L	High Class III	Substance would not be expected to be a safety concern	Negative for nongenotoxic carcinogenicity
Mauritine-M	High Class III	Substance would not be expected to be a safety concern	Negative for nongenotoxic carcinogenicity

properties of these compounds, intended for consideration as novel drug candidates. Various parameters were utilized in toxicity prediction, including Cramer Rules, aimed at evaluating toxicity levels based on functional groups, Kroes TTC, utilized for estimating human exposure thresholds concerning the Mauritine compounds, and Carcinogenicity, which assesses the potential of the Mauritine compounds to induce carcinogenicity and mutagenicity. The outcomes of the Mauritine compound's toxicity prediction are qualitative, determining whether the compound exhibits toxic properties.

The toxicity assessment outcomes depicted in Table 2 reveal that all Mauritine compounds fall under class III toxicity, indicating their high toxicity level as per the Cramer Rules parameters. However, based on the Kroes TTC parameters, the Mauritine compounds do not surpass the intake limit for human exposure concerning the Mauritine compounds. Furthermore, the Carcinogenicity parameters indicate that Mauritine derivative compounds do not induce carcinogenicity or mutagenicity.

3.3. Refinement of the geometric structure of Mauritine compounds

Geometry optimization was conducted aiming to acquire the most stable conformation of the Mauritine compound structure, facilitating its potential binding to the active site of the macromolecular receptor during the subsequent molecular docking simulation. This optimization process was executed using Quantum ESPRESSO v.6.6 software, yielding outcomes in the form of the lowest total energy values (Table 3).

The lowest total energy signifies the achievement of optimal structural stability. Among the Mauritine compounds examined, the data from the lowest total energy analysis highlights that Mauritine-D demonstrates the smallest total energy compared to the remaining compounds. This observation indicates that the structural conformation of the Mauritine-D compound attains a notably higher level of stability compared to the other eight Mauritine compounds.

3.4. Validation of the molecular docking method

Prior to validating the docking method, the papain-like protease receptor (PLpro) underwent preparation using Biovia Discovery Studio 2019 software. This preparation involved the elimination of water molecules and segregation of the natural ligand from the macromolecules. The elimination of water molecules serves to prevent interference in the

Table 3. The total energy derived from the geometric optimization of the Mauritine compounds.

Compound	Total energy
Mauritine-A	-0.1481 a.u.
Mauritine-B	-0.1881 a.u.
Mauritine-C	-0.1001 a.u.
Mauritine-D	-0.2423 a.u.
Mauritine-F	-0.1780 a.u.
Mauritine-H	-0.1835 a.u.
Mauritine-J	-0.1653 a.u.
Mauritine-L	-0.1615 a.u.
Mauritine-M	-0.2199 a.u.

Table 4. Validation parameters for the molecular docking method.

Parameter	Result
Grid box	X: 64; Y: 60; Z: 60
Spacing	0.375
Grid center	X: -33.866; Y: -11.293; Z: 30.009
RMSD	1.91 Å
Binding Free Energy	-9.96 Kcal/mol
Inhibition Constant	0.05 µM (micromolar)

Table 5. Results obtained from molecular docking simulations encompass the binding free energy and inhibition constant.

Compound	Binding free energy (Kcal/mol)	Inhibition constant [µM (micromolar)]
Native (GRL0617)	-9.96	0.05
Mauritine-A	-8.58	0.51724
Mauritine-B	-7.73	2.14
Mauritine-C	-8.36	0.7398
Mauritine-D	-6.07	35.43
Mauritine-F	-6.67	12.95
Mauritine-H	-7.83	1.83
Mauritine-J	-7.67	2.38
Mauritine-L	-7.40	3.80
Mauritine-M	-6.87	9.17

molecular docking process. Subsequently, the process included the addition of hydrogen atoms to fulfill incomplete hydrogen bonds within the receptor structure at the time of download. Concurrently, the addition of partial charges aimed to neutralize the charge present on the receptor macromolecules.

The primary objective of this docking method validation is to fine-tune the method to ensure precise docking by utilizing the Root Mean Square Deviation (RMSD) parameter. A validated docking method is indicated by an RMSD value of ≤ 2 Å. The validation outcomes presented in Table 4 confirm the reliability of the employed method, given the RMSD value of 1.91 Å, falling within the acceptable range of ≤ 2 Å (Mahtarin et al., 2022). The RMSD value delineates the

conformational alignment of the natural ligand concerning its initial position before re-docking. A lower RMSD value signifies greater accuracy, indicating a closer alignment of the ligand within the receptor's active site.

3.5. Simulation of molecular docking for Mauritine compounds

Molecular docking serves as a computational simulation aimed at foreseeing the configuration of the complex formed between the receptor and the ligand. Outcomes derived from the docking process include the binding free energy and inhibition constant, serving as indicators of the conformational stability between the Mauritine compound and the PLpro receptor. Stable interactions typically generate lower binding free energies. Binding free energy signifies the capacity of a compound or drug to attach to a receptor, where smaller bond energies signify heightened affinity between the ligand and the receptor (Table 5).

As indicated by molecular docking simulations, it is anticipated that among the nine Mauritine compounds, Mauritine-A and Mauritine-C exhibits the most favorable binding free energy. This indicates a stable interaction between the Mauritine-A and Mauritine-C compound and the PLpro receptor within the active site. Furthermore, in terms of the inhibition constant value, Mauritine-A and Mauritine-C demonstrates the lowest value among the other seven compounds. This underscores the effective inhibitory potential of the Mauritine-A and Mauritine-C compound against the PLpro receptor.

3.6. Evaluation of the outcomes from the molecular docking simulations

The analysis of the molecular docking results aimed to assess the inhibition achieved by the utilized Mauritine compounds. Illustrated in Figure 3, this outcome presents the interactions established between amino acid residues and the Mauritine compounds. These interactions between amino acids facilitate the contact between the ligand and the receptor, contributing to the inhibitory activity and binding energy within the active binding site. This active site, crucial for the ligand-receptor binding, significantly influences the receptor's conformation and functionality. Furthermore, within this active site, specific amino acid residues play a pivotal role in forming various interactions, including hydrogen bonds, hydrophobic interactions, and electrostatic interactions, crucial for the ligand-receptor association (Kumar et al., 2022).

However, among the nine Mauritine compounds studied through molecular docking simulation analysis, Mauritine-H appears to exhibit the highest level of molecular interaction. This specific compound exhibits a greater ability to bind with amino acid residues in comparison to the other Mauritine compounds. Mauritine-H manifests 16 interactions with the PLpro receptor's binding active site, encompassing 4 hydrogen bonds (involving Thr301, Pro247, Pro248, and Asp302), 1 electrostatic interaction (with Arg166), and 11 hydrophobic interactions (involving Tyr264, Tyr268, Pro247,

Pro248, Tyr264, Tyr264, Tyr268, Tyr268, Pro247, and Pro248). Such extensive interactions signify a notably stable and robust bond formed with the PLpro receptor. Additionally, other Mauritine compounds, including Mauritine-M (demonstrating 11 interactions), Mauritine A, and Mauritine-B (both exhibiting 10 interactions), also exhibit similar binding abilities akin to Mauritine-H.

On the other hand, among the Mauritine compounds, Mauritine-L and Mauritine-J demonstrated the least robust interactions within the PLpro receptor binding active site, establishing 5 and 6 interactions, respectively. Specifically, Mauritine-L formed interactions solely with amino acid residues Pro248, Tyr268, Glu167, Arg166, and Pro247. Conversely, Mauritine-J interacted with amino acid residues Asp164, Gln269, Glu167, Arg166, Leu162, and Arg166. The observations from Table 6 suggest that all amino acid residues engaged in interactions with the Mauritine compounds serve as integral components of the active site within the PLpro receptor, thereby being vital for its functionality as a targeted macromolecule.

3.7. Simulation of molecular dynamics for Mauritine compounds

The superior compounds identified through molecular docking proceeded to undergo molecular dynamics simulations. A 500 ns simulation was conducted on the native—PLpro, Mauritine-A—PLpro, and Mauritine-C—PLpro complexes. The stability assessment of the complex system was performed by analyzing RMSD, RMSF, and MM-PBSA binding free energy. The RMSD trajectory of the entire complex system was computed over the 500 ns simulation. A comparison was made among the RMSD values of the native ligand (GRL0617), Mauritine-A, and Mauritine-C complexes. The RMSD trajectory plot among these three complexes (depicted in Figure 4) demonstrated analogous results from the initial phase of the simulation at 0 ns to 30 ns. However, noticeable discrepancies in fluctuations emerged between 100 ns to 350 ns. In the Mauritine-A—PLpro and Mauritine-C—PLpro complexes, the RMSD of the complex remained lower, within the range of 0.10 nm to 0.15 nm, while the native—PLpro complex showed values in the range of 0.15 nm to 0.20 nm. Subsequently, all three complexes exhibited a convergence to similar RMSD values at 350 ns until the culmination of the 500 ns simulation. During the latter part of the simulation, from 450 ns to 500 ns, there was an escalation in fluctuations observed in the native complex (GRL0617), reaching around 0.25 nm to 0.30 nm.

In contrast, the RMSF value reveals a substantial similarity in interactions among the three complexes, except for specific amino acid sequences: 180–200 and 250–270. During this period, the RMSF fluctuations observed in the native—PLpro and Mauritine-C—PLpro complexes were more pronounced compared to those in the Mauritine-A—PLpro complex (Figure 5). The rise in RMSF fluctuations observed in both complexes signifies an escalated variability in interactions within a specific sequence of amino acids. Conversely, the Mauritine-A—PLpro complex exhibited enhanced stability regarding RMSF

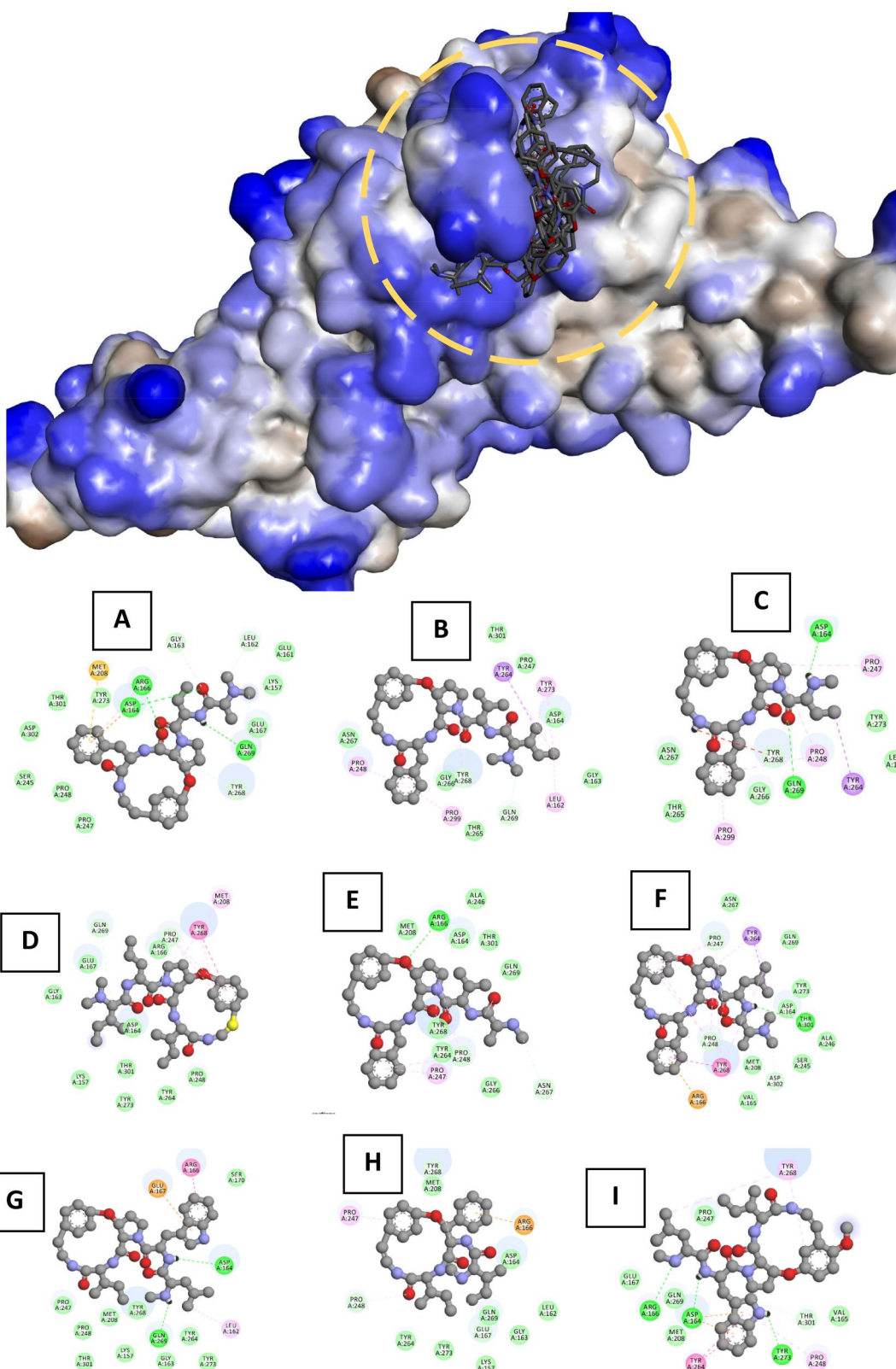


Figure 3. The molecular interactions established between the PLpro receptor and compounds Mauritine-A (A), Mauritine-B (B), Mauritine-C (C), Mauritine-D (D), Mauritine-F (E), Mauritine-H (F), Mauritine-J (G), Mauritine-L (H), and Mauritine-M (I).

fluctuations across the same range of amino acids. These distinctions signify the existence of diverse potential interactions within the molecules under scrutiny, emphasizing the influence of candidate compounds on the dynamics of protein-ligand complexes (Ramadhan et al., 2022).

In the observation of the RMSF graph, there are several amino acid residues that experience a decrease during molecular dynamics simulation compared to the amino acid residues during molecular docking. This phenomenon can occur due to the stronger interactions between the target

Table 6. Interactions occurring among amino acid residues within the binding active site of the PLpro receptor.

Compound	Number of interaction	Amino acid residue
Mauritine-A	10	Asp164, Arg166, Arg166, Gln269, Gly163, Tyr268, Leu162, Gln269, Asp164, Arg166
Mauritine-B	10	Tyr268, Gln269, Tyr264, Leu162, Tyr264, Tyr268, Tyr273, Tyr273, Pro248, Pro299
Mauritine-C	8	Gln269, Asp164, Tyr268, Tyr264, Pro247, Pro248, Pro248, Pro299
Mauritine-D	7	Pro247, Gln269, Tyr268, Pro247, Met208, Tyr268, Pro247
Mauritine-F	7	Arg166, Pro248, Asn267, Pro247, Pro248, Pro247, Pro248
Mauritine-H	16	Thr301, Pro247, Pro248, Asp302, Arg166, Tyr264, Tyr268, Pro247, Pro248, Pro248, Tyr264, Tyr264, Tyr268, Tyr268, Pro247, Pro248
Mauritine-J	6	Asp164, Gln269, Glu167, Arg166, Leu162, Arg166
Mauritine-L	5	Pro248, Tyr268, Glu167, Arg166, Pro247
Mauritine-M	11	Arg166, Asp164, Tyr273, Thr301, Asp164, Asp164, Tyr264, Tyr264, Tyr268, Tyr268, Pro248

Description: Hydrogen Bonds (Indicated in Green), Electrostatic Interactions (Marked in Yellow), Hydrophobic Interactions (Highlighted in Red).

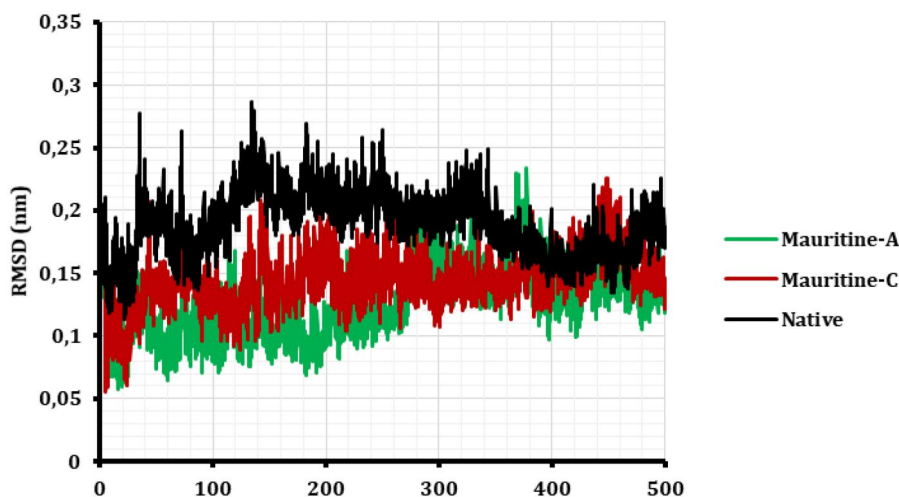


Figure 4. A visual depiction illustrating the stability analysis of the complex through RMSD values is presented graphically. The RMSD values corresponding to the native—PLpro complex are depicted in black, while those for the Mauritine-A—PLpro complex are visualized in green, and the RMSD values for the Mauritine-C—PLpro complex are represented in red.

molecule and the drug molecule during dynamic simulation. Additionally, molecular dynamics simulation provides a more realistic portrayal of conformational changes and molecular dynamics during interactions, which may not be apparent during static molecular docking. This suggests that the drug molecule may more effectively interact with the target at the atomic level during dynamic simulations, opening opportunities for further developments in drug design and understanding interaction mechanisms (Hikmawati et al., 2022).

3.8. Calculation of binding free energy using MM-PBSA

The MM-PBSA method was utilized to compute the binding free energy throughout a 500 ns simulation, generating 500 snapshot trajectories. Comparing the binding free energy among the three complexes, it's evident that both the Mauritine-A and Mauritine-C complexes exhibit binding free energy values close to their respective native ligand complexes (GRL0617) (Table 7). Across all three complexes, positive values denote polar solvation energy (KJ/mol), while the rest exhibit negative energy values. The native ligand complex (GRL0617) demonstrates higher energy values in terms of van de Waals energy (KJ/mol), electrostatic energy (KJ/mol), and SASA energy (KJ/mol). Variations in binding energy

between molecular docking and dynamics results stem from fluctuating changes induced by Mauritine-A and Mauritine-C in simulations. Conversely, molecular docking renders the protein in a rigid state, leading to unpredictable protein fluctuations. Since the binding free energy of compounds Mauritine-A and Mauritine-C exceeded that of the native ligand in PLpro (GRL0617), they exhibited potential activity in the in silico analysis, demonstrating superior binding free energy compared to the native ligand (GRL0617).

4. Conclusions

Through molecular docking simulations, it's evident that all nine Mauritine compounds interact with the papain-like protease (PLpro) receptor. Among these, Mauritine-A (binding free energy of -8.58 Kcal/mol and an inhibition constant of $0.51724 \mu\text{M}$) and Mauritine-C (binding free energy of -8.36 Kcal/mol and an inhibition constant of $0.7398 \mu\text{M}$) exhibits superior affinity, surpassing other Mauritine compounds. Further affirmed by molecular dynamics simulations, the stability demonstrated by Mauritine-A and Mauritine-C is evident in its RMSD and RMSF values. Calculations of MM-PBSA binding free energy place the Mauritine-A and Mauritine-C compounds at -162.431 kJ/mol and -137.500 kJ/mol, respectively.

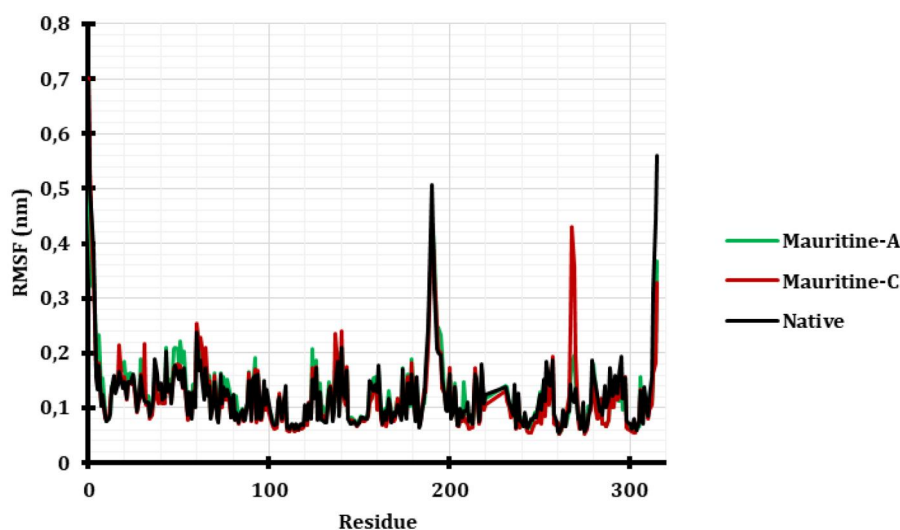


Figure 5. A graphical representation displaying the assessment of stability within the complex using RMSF values is provided. The RMSF values of the native—PLpro complex are portrayed in black, the Mauritine-A—PLpro complex is depicted in green, and the RMSF values pertaining to the Mauritine-C—PLpro complex are illustrated in red.

Table 7. The condensed results obtained from the MM-PBSA analysis provide significant insights into both the total binding energy and its individual components.

Complex	ΔE_{vdw} (kJ/mol)	ΔE_{ele} (kJ/mol)	ΔG_{PB} (kJ/mol)	ΔG_{NP} (kJ/mol)	ΔG_{Bind} (kJ/mol)
Native—PLpro	−152.926	−46.597	123.674	−15.715	−91.564
Mauritine-A—PLpro	−145.761	−56.673	46.020	−6.017	−162.431
Mauritine-C—PLpro	−118.813	−54.122	37.475	−2.040	−137.500

Note: ΔE_{vdw} = van der Waals contribution, ΔE_{ele} = electrostatic contribution, ΔG_{PB} = polar contribution of desolvation, ΔG_{NP} = non-polar contribution of desolvation, ΔG_{Bind} = binding-free energy.

As a result, Mauritine-A and Mauritine-C emerges as a promising antiviral candidate, particularly against SARS-CoV-2.

Acknowledgment

The author extends gratitude to the Department of Pharmacy, Faculty of Mathematics and Natural Sciences, Universitas Islam Bandung, for their financial support granted through the 2020 Independent Research program under No. 03/PEN-PKM/I/2021.

Disclosure statement

The authors declare no conflict of interest.

Funding

This research received no external funding.

ORCID

Taufik Muhammad Fakhri <http://orcid.org/0000-0001-7155-4412>
 Fitrianti Darusman <http://orcid.org/0000-0003-3300-9231>
 Dwi Syah Fitra Ramadhan <http://orcid.org/0000-0001-6257-7276>
 Aulia Fikri Hidayat <http://orcid.org/0000-0001-5111-8613>
 Aden Dhana Rizkita <http://orcid.org/0000-0002-8979-0234>
 Tegar Achsendo Yuniarta <http://orcid.org/0000-0002-5326-7636>

Author contributions

Conceptualization, T.M.F., F.D., and D.S.F.R.; methodology, T.M.F., D.S.F.R., and T.A.Y.; software, T.M.F., D.S.F.R., A.F.H., A.D.R., and T.A.Y.; validation, R.A., and S.P.; formal analysis, R.A., and S.P.; investigation, R.A., and S.P.;

resources, R.A., and S.P.; data curation, R.A., and S.P.; writing—original-draft preparation, R.A., and S.P.; writing—review and editing, T.M.F., F.D., D.S.F.R., A.F.H., A.D.R., and T.A.Y.; visualization, R.A., and S.P.; supervision, T.M.F., F.D., D.S.F.R., and T.A.Y.; All authors have read and agreed to the published version of the manuscript.

References

- Abraham, M., Hess, B., D van der, S., & Lindahl, E. (2015). The GROMACS development team, GROMACS user manual. *Version*, 5(0.7).
- Adam IA, Irshad R, Atia-tul-Wahab, Omoboyowa DA, Choudhary MI, Wang Y. Two new 5(14)-membered type cyclopeptide alkaloids from root bark of *Ziziphus spina-christi* (L.) Desf. *Natural Product Research*. 2023;37(15), 2473–2479. <https://doi.org/10.1080/14786419.2022.2050227>
- Anand, K. B., Karade, S., Sen, S., & Gupta, R. M. (2020). SARS-CoV-2: Camazotz's curse. *Medical Journal, Armed Forces India*, 76(2), 136–141. <https://doi.org/10.1016/j.mjafi.2020.04.008>
- Aragones, J. L., Noya, E. G., Valeriani, C., & Vega, C. (2013). Free energy calculations for molecular solids using GROMACS. *The Journal of Chemical Physics*, 139(3), 034104. <https://doi.org/10.1063/1.4812362>
- Armstrong, L. A., Lange, S. M., Dee Cesare, V., Matthews, S. P., Nirujogi, R. S., Cole, I., Hope, A., Cunningham, F., Toth, R., Mukherjee, R., Bojkova, D., Gruber, F., Gray, D., Wyatt, P. G., Cinatl, J., Dikic, I., Davies, P., & Kulathu, Y. (2021). Biochemical characterization of protease activity of Nsp3 from SARS-CoV-2 and its inhibition by nanobodies. *PLoS One*, 16(7), e0253364. <https://doi.org/10.1371/journal.pone.0253364>
- Arya, R., Prashar, V., & Kumar, M. (2022). Evaluating stability and activity of SARS-CoV-2 PLpro for high-throughput screening of inhibitors. *Molecular Biotechnology*, 64(1), 1–8. <https://doi.org/10.1007/s12033-021-00383-y>
- Az-Zahra, F., Afidika, J., Diamantha, S. D. A., Rahmani, A. E., Fatimah, S., Aulifa, D. L., Elaine, A. A., & Sitinjak, B. D. P. (2022). Indonesian journal of biological pharmacy in silico study of betel leaves compound (Piper betle L.) as acetylcholinesterase (AChE) enzyme inhibitor in Alzheimer Disease. *Indonesian Journal of Biological Pharmacy*, 2(2), 44. <https://doi.org/10.24198/ijbp.v2i2.40462>

- Bhowmick, S., AlFaris, N. A., Zaidan ALTamimi, J., AlOthman, Z. A., Patil, P. C., Aldayel, T. S., Wabaidur, S. M., & Saha, A. (2022). Identification of bio-active food compounds as potential SARS-CoV-2 PLpro inhibitors-modulators via negative image-based screening and computational simulations. *Computers in Biology and Medicine*, *145*, 105474. <https://doi.org/10.1016/j.combiomed.2022.105474>
- BIOVIA. (2017). *Dassault Systèmes BIOVIA, discovery studio modeling environment, release 2017*. San Diego, CA: Dassault Systèmes.
- Daina, A., Michielin, O., & Zoete, V. (2017). SwissADME: A free web tool to evaluate pharmacokinetics, drug-likeness and medicinal chemistry friendliness of small molecules. *Scientific Reports*, *7*(1), 42717. <https://doi.org/10.1038/srep42717>
- Djajadisastra, J., Purnama, H. D., & Yanuar, A. (2017). In silico binding interaction study of mefenamic acid and piroxicam on human albumin. *International Journal of Applied Pharmaceutics*, *9*, 102. https://doi.org/10.22159/ijap.2017.v9s1.56_62
- Fakih, T. M., Putri, N. W. R. P., Marillia, V., Ramadhan, D. S. F., & Darusman, F. (2022). Identifikasi Aktivitas Biologis, Prediksi Toksisitas, dan Molecular Docking Senyawa Jubanine dari Tanaman Bidara Arab sebagai Kandidat Antivirus SARS-CoV-2. *J Ris Kim*, *13*(1) <https://doi.org/10.25077/jrk.v13i1.437>
- Farooq Wali, A., Ramakrishna Pillai, J., Beigh, S., Mushtaq, A., Arafah, A., Rehman, M. U., Jabnoun, S., Razmpoor, M., Al Dibsawi, A., Alshehri Resource, S., Ghoneim, M. M., & Sarim Imam, S. (2022). Ethnopharmacological uses, phytochemistry, pharmacological properties and clinical trials of Ziziphus Spina-Christi: A comprehensive review. *Saudi Pharmaceutical Journal*, <https://doi.org/10.1016/j.jsps.2022.05.001>
- Forli, W., Halliday, S., Belew, R., & Olson, A. (2012). AutoDock Version 4.2. Citeseer.
- Gao, X., Qin, B., Chen, P., Zhu, K., Hou, P., Wojdyla, J. A., Wang, M., & Cui, S. (2021). Crystal structure of SARS-CoV-2 papain-like protease. *Acta Pharmaceutica Sinica B*, *11*(1), 237–245. <https://doi.org/10.1016/j.apsb.2020.08.014>
- Giannozzi, P., Barone, O., Bonfà, P., Brunato, D., Car, R., Carnimeo, I., Cavazzoni, C., de Gironcoli, S., Delugas, P., Ferrari Ruffino, F., Ferretti, A., Marzari, N., Timrov, I., Urru, A., & Baroni, S. (2020). Quantum ESPRESSO toward the exascale. *The Journal of Chemical Physics*, *152*(15), 154105. <https://doi.org/10.1063/5.0005082>
- Guo, Y.-R., Cao, Q.-D., Hong, Z.-S., Tan, Y.-Y., Chen, S.-D., Jin, H.-J., Tan, K.-S., Wang, D.-Y., & Yan, Y. (2020). The origin, transmission and clinical therapies on coronavirus disease 2019 (COVID-19) outbreak: A n update on the status. *Military Medical Research*, *7*(1). <https://doi.org/10.1186/s40779-020-00240-0>
- Hikmawati, D., Fakih, T. M., Sutedia, E., Dwiyanita, R. F., Atik, N., & Ramadhan, D. S. F. (2022). Pharmacophore-guided virtual screening and dynamic simulation of Kallikrein-5 inhibitor: Discovery of potential molecules for rosacea therapy. *Informatics in Medicine Unlocked*, *28*, 100844. <https://doi.org/10.1016/j.imu.2022.100844>
- Karami, T. K., Hailu, S., Feng, S., Graham, R., & Gukasyan, H. J. (2022). Eyes on Lipinski's rule of five: A new "rule of thumb" for physico-chemical design space of ophthalmic drugs. *Journal of Ocular Pharmacology and Therapeutics: The Official Journal of the Association for Ocular Pharmacology and Therapeutics*, *38*(1), 43–55. <https://doi.org/10.1089/jop.2021.0069>
- Khan, R. J., Jha, R. K., Singh, E., Jain, M., Amera, G. M., Singh, R. P., et al. (2022). Identification of promising antiviral drug candidates against non-structural protein 15 (NSP15) from SARS-CoV-2: An in silico assisted drug-repurposing study. *Journal of Biomolecular Structure and Dynamics*. *40*(1). <https://doi.org/10.1080/07391102.2020.1814870>
- Kidaka, T., Lokupathirage, S. M. W., Muthusinghe, B. D. S., Pongombo, B. L., Wastika, C. E., Wei, Z., et al. (2020). Review on counter measures to coronavirus disease 2019 (COVID-19) pandemic, May 2020. *Japanese Journal of Veterinary Research*. *68*(3). <https://doi.org/10.14943/jjvr.68.3.133>
- Kim, S., Chen, J., Cheng, T., Gindulyte, A., He, J., He, S., Li, Q., Shoemaker, B. A., Thiessen, P. A., Yu, B., Zaslavsky, L., Zhang, J., & Bolton, E. E. (2023). PubChem 2023 update. *Nucleic Acids Research*, *51*(D1), D1373–D1380. <https://doi.org/10.1093/nar/gkac956>
- Kumar, N., Kaur, K., & Bedi, P. M. S. (2023). Hybridization of molecular docking studies with machine learning based QSAR model for prediction of xanthine oxidase activity. *Computational and Theoretical Chemistry*. *1227*, 114262. <https://doi.org/10.1016/j.comptc.2023.114262>
- Kumar, N., Singh, A., Gulati, H. K., Bhagat, K., Kaur, K., Kaur, J., Dudhal, S., Duggal, A., Gulati, P., Singh, H., Singh, J. V., & Bedi, P. M. S. (2021). Phytoconstituents from ten natural herbs as potent inhibitors of main protease enzyme of SARS-COV-2: In silico study. *Phytomedicine plus: International Journal of Phytotherapy and Phytopharmacology*, *1*(4), 100083. <https://doi.org/10.1016/j.phyplu.2021.100083>
- Kumar, N., Singh, J. V., Bhagat, K., Gulati, H. K., Sharma, A., Rani, A., Duggal, A., Gulati, P., Singh, H., Bedi, P. M. S., & Kaur, S. (2022). Discovery of potent inhibitors for Mpro enzyme of SARS-COV2 by multi-stage in-silico screening of Alkannin/shikonin. *Natural Product Research*, *36*(18), 4804–4808. <https://doi.org/10.1080/14786419.2021.2013212>
- Li, H., Chen, C., Hu, F., Wang, J., Zhao, Q., Gale, R. P., & Liang, Y. (2020). Impact of corticosteroid therapy on outcomes of persons with SARS-CoV-2, SARS-CoV, or MERS-CoV infection: A systematic review and meta-analysis. *Leukemia*, *34*(6), 1503–1511. <https://doi.org/10.1038/s41375-020-0848-3>
- Liu, Q., Lu, P., Shen, Y., Li, C., Wang, J., Zhu, L., Lu, W., & Martinez, L. (2021). Collateral impact of the coronavirus disease 2019 (COVID-19) pandemic on tuberculosis control in Jiangsu Province, China. *Clinical Infectious Diseases: An Official Publication of the Infectious Diseases Society of America*, *73*(3), 542–544. <https://doi.org/10.1093/cid/cia1289>
- Lohidakshan, K., Rajan, M., Ganesh, A., Paul, M., & Jerin, J. (2018). Pass and Swiss ADME collaborated in silico docking approach to the synthesis of certain pyrazoline spacer compounds for dihydrofolate reductase inhibition and antimalarial activity. *Bangladesh Journal of Pharmacology*, *13*(1), 23. <https://doi.org/10.3329/bjpv.v13i1.33625>
- Mahtarin, R., Islam, S., Islam, M. J., Ullah, M. O., Ali, M. A., & Halim, M. A. (2022). Structure and dynamics of membrane protein in SARS-CoV-2. *Journal of Biomolecular Structure and Dynamics*. *40*(10), 4725–4738. <https://doi.org/10.1080/07391102.2020.1861983>
- Mohamed, K., Rzymiski, P., Islam, M. S., Makuku, R., Mushtaq, A., Khan, A., Ivanovska, M., Makka, S. A., Hashem, F., Marquez, L., Cseprekal, O., Filgueiras, I. S., Fonseca, D. L. M., Mickael, E., Ling, I., Arero, A. G., Cuschieri, S., Minakova, K., Rodriguez-Román, E., ... Rezaei, N. (2022). COVID-19 vaccinations: The unknowns, challenges, and hopes. *Journal of Medical Virology*, *94*(4), 1336–1349. <https://doi.org/10.1002/jmv.27487>
- Moreno-Eutimio, M. A., López-Macías, C., & Pastelin-Palacios, R. (2020). Bioinformatic analysis and identification of single-stranded RNA sequences recognized by TLR7/8 in the SARS-CoV-2, SARS-CoV, and MERS-CoV genomes. *Microbes and Infection*, *22*(4-5), 226–229. <https://doi.org/10.1016/j.micinf.2020.04.009>
- Muchtaridi, M., Triwahyuningtyas, D., Muhammad Fakih, T., Megantara, S., & Choi, S. B. (2023). Mechanistic insight of α -mangostin encapsulation in 2-hydroxypropyl- β -cyclodextrin for solubility enhancement. *Journal of Biomolecular Structure & Dynamics*, 1–10. <https://doi.org/10.1080/07391102.2023.2214237>
- Mulyani, S., Adriani, M., & Wirjatmadi, B. (2021). Antibacterial activity of extract ethanol bidara leaves (Ziziphus spina-christi l) on enteropathogenic coli. *Indian Journal of Forensic Medicine & Toxicology*, *15*(1). <https://doi.org/10.37506/ijfvt.v15i1.13638>
- Ramadhan, D. S. F., Siharis, F., Abdurrahman, S., Isrul, M., & Fakih, T. M. (2022). In silico analysis of marine natural product from sponge (Clathria Sp.) for their activity as inhibitor of SARS-CoV-2 Main Protease. *Journal of Biomolecular Structure and Dynamics*. *40*(22), 11526–11532. <https://doi.org/10.1080/07391102.2021.1959405>
- Ren, J., Yuan, X., Li, J., Lin, S., Yang, B., Chen, C., Zhao, J., Zheng, W., Liao, H., Yang, Z., & Qu, Z. (2020). Assessing the performance of the g_mmpbsa tools to simulate the inhibition of oseltamivir to influenza virus neuraminidase by molecular mechanics Poisson–Boltzmann surface area methods. *Journal of the Chinese Chemical Society*, *67*(1), 46–53. <https://doi.org/10.1002/jccs.201900148>
- Sakna, S. T., Mocan, A., Sultani, H. N., El-Fiky, N. M., Wessjohann, L. A., & Farag, M. A. (2019). Metabolites profiling of Ziziphus leaf taxa via UHPLC/PDA/

- ESI-MS in relation to their biological activities. *Food Chemistry*, 293, 233–246. <https://doi.org/10.1016/j.foodchem.2019.04.097>
- Shen, C.-H., Tie, Y., Yu, X., Wang, Y.-F., Kovalevsky, A. Y., Harrison, R. W., & Weber, I. T. (2012). Capturing the reaction pathway in near-atomic-resolution crystal structures of HIV-1 protease. *Biochemistry*, 51(39), 7726–7732. <https://doi.org/10.1021/bi3008092>
- Smith, M. D., Rao, J. S., Segelken, E., & Cruz, L. (2015). Force-field induced bias in the structure of A β 21–30: A comparison of OPLS, AMBER, CHARMM, and GROMOS force fields. *Journal of Chemical Information and Modeling*, 55(12), 2587–2595. <https://doi.org/10.1021/acs.jcim.5b00308>
- Sokolinskaya, E. L., Putlyaeva, L. V., Polinovskaya, V. S., & Lukyanov, K. A. (2022). Genetically encoded fluorescent sensors for SARS-CoV-2 papain-like protease PLpro. *International Journal of Molecular Sciences*, 23(14), 7826. <https://doi.org/10.3390/ijms23147826>
- Sousa Da Silva, A. W., & Vranken, W. F. (2012). ACPYPE: AnteChamber PYthon parser interface. *BMC Research Notes*, 5(1). <https://doi.org/10.1186/1756-0500-5-367>
- Taghipour, M. T., Nameni, R., Taghipour, M., & Ghorat, F. (2020). Phytochemical analysis and antimicrobial activity of Ziziphus spina-christi and Tamarix aphylla Leaves' extracts as effective treatment for coronavirus disease 2019 (COVID-19). *Thrita*, 9(2). <https://doi.org/10.5812/thrita.107776>
- Tallei, Trina Ekawati, Yelnetty, Afriza, Idroes, Rinaldi, Kusumawaty, Diah, Emran, Talha Bin, Yesiloglu, Talha Zahid, Sippl, Wolfgang, Mahmud, Shafi, Alqahtani, Taha, Alqahtani, Ali M, Asiri, Saeed, Rahmatullah, Mohammed, Jahan, Rowan, Khan, Md Arif, Celik, Ismail, Fatimawali .. An analysis based on molecular docking and molecular dynamics simulation study of Bromelain as anti-SARS-CoV-2 variants. *Frontiers in Pharmacology*, 717757. 2021;12. <https://doi.org/10.3389/fphar.2021.717757>
- Tsai, Y. C., Chen, W. Y., & Chiu, C. C (2023). Molecular effects of site-specific phosphate-methylated primer on the structure and motions of Taq DNA polymerase. *Computational and Structural Biotechnology Journal*. 21. <https://doi.org/10.1016/j.csbj.2023.02.043>
- Tuenter, E., Foubert, K., Staerk, D., Apers, S., & Pieters, L. (2017). Isolation and structure elucidation of cyclopeptide alkaloids from Ziziphus nummularia and Ziziphus spina-christi by HPLC-DAD-MS and HPLC-PDA-(HRMS)-SPE-NMR. *Phytochemistry*, 138, 163–169. <https://doi.org/10.1016/j.phytochem.2017.02.029>
- Velayati, A., Farnia, P., Besharati, S., Farnia, P., & Ghanavi, J. (2020). The importance of genomic changes of SARS-CoV-2 and its comparison with Iranian-reported COVID-19 sequencing; whether each country has to design its treatment and vaccine production. *Biomedical and Biotechnology Research Journal*, 4. https://doi.org/10.4103/bbrj.bbrj_122_20
- Walls, A. C., Park, Y. J., Tortorici, M. A., Wall, A., McGuire, A. T., & Velesler, D. (2020). Structure, function, and antigenicity of the SARS-CoV-2 spike glycoprotein. *Cell*, 181(2), 281–292.e6. <https://doi.org/10.1016/j.cell.2020.02.058>
- Wang, C., Greene, D., Xiao, L., Qi, R., & Luo, R. (2017). Recent developments and applications of the MMPBSA method. *Frontiers in Molecular Biosciences*, 4, 87. <https://doi.org/10.3389/fmolb.2017.00087>
- Yang, L. L., & Yang, T. (2020). Pulmonary rehabilitation for patients with coronavirus disease 2019 (COVID-19). *Chronic Diseases and Translational Medicine*, 6(2), 79–86. <https://doi.org/10.1016/j.cdtm.2020.05.002>
- Yang, X., Chen, X., Bian, G., Tu, J., Xing, Y., Wang, Y., & Chen, Z. (2014). Proteolytic processing, deubiquitinase and interferon antagonist activities of Middle East respiratory syndrome coronavirus papain-like protease. *Journal of General Virology*, 95(3), 614–626. <https://doi.org/10.1099/vir.0.059014-0>
- Yeni, Y., Supandi, S., & Merdekawati, F. (2018). In silico toxicity prediction of 1-phenyl-1-(quinazolin-4-yl) ethanol compounds by using Toxtree, pkCSM and preADMET. *Pharmaciana*, 8(2), 216. <https://doi.org/10.12928/pharmaciana.v8i2.9508>